Articles
doi.org/10.1002/batt.202000255

Chemistry Europe
European Chemical Societies Publishing

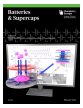

A New Cell Configuration for a More Precise Electrochemical Evaluation of an Artificial Solid-Electrolyte Interphase

Jernej Bobnar,[a, b] Alen Vizintin,[a] Gregor Kapun,[a] Christian Njel,[c, d] Rémi Dedryvère,[c, d] Robert Dominko,*[a, b, d] and Bostjan Genorio*[b]

The study of an artificial solid-electrolyte interphase (SEI) can lead to a misinterpretation of the electrochemical results obtained with the classical cell configuration due to so-called edge effect. A technical solution is presented here that minimizes the edge effect by using a new cell configuration with a polypropylene disc. A new cell configuration allows a simple electrochemical evaluation of an artificial SEI with a more precisely defined effective area and homogeneously distributed current density. The application of such a technical solution manifests itself through better defined deposition and stripping curves in relation to surface electrochemistry and can differ significantly from the results obtained with the classical cell configuration. Finally, a model system - a lithium electrode protected with trimethylolpropane ethoxylate triacrylate polymer-was used to evaluate and compare the new cell configuration with the classical two electrode cell configuration.

1. Introduction

Lithium metal batteries (LMB) offer a significant increase in theoretical energy density compared to current lithium-ion (Li-ion) battery technology and are therefore considered the next generation of batteries. The increase in energy density is therefore mainly due to the high specific energy (3860 mAh g^{-1}), the low density (0.534 g cm^{-2}) and the lowest standard reduction potential (−3.040 V vs. SHE) of lithium metal.[1,2]

Unfortunately, several difficulties are hampering the commercialization of LMB, the most prominent of which is related to the lithium metal (e.g. low Coulombic efficiency accompanied with lithium degradation and electrolyte consumption, low safety). The root of the problems with the lithium metal lies in two of its properties: a) high reactivity (electropositivity) of the lithium metal, and b) infinite host-less volume change. The combination of both properties leads to reactions between lithium metal and electrolyte forming a heterogeneous solid–electrolyte interphase (SEI), to its cracking and to the formation of preferred areas for lithium deposition i.e. dendritic growth.[3,4] In relation to the dendritic growth, remarkable improvements have recently been made towards safer and more stable lithium metal electrodes. Although numerous solutions have been proposed, such as reformulations of the electrolyte,[5,6] modification of separators,[7,8] and modifications of the surface of lithium metal electrode,[9–11] there is still no unambiguous solution that would effectively suppress formation of high surface area lithium (HSAL). One of the proposed solutions is the formation of an artificial SEI. Artificial SEI can be prepared by engineering the surface of the lithium electrode by using various materials such as porous carbons,[12,13] polymers,[14–17] ceramic layers,[18–20] and inorganic-organic composite,[21,22] that can impact Li-ion conductivity and Li-ion flow homogeneity. The most conspicuous problem with such engineered electrodes is the lithium deposition can occur at the preferred locations. It has been shown previously that lithium is preferably deposited locally near the edges of the electrode and electrode tab due to the local voltage drop below 0 V versus Li/Li^+[23–26] or where pressure of the cell is lower[27] or locally near of the defects in the separator.[28] Previously, the preferred deposition at the edges of the electrodes (edge effect) was usually only addressed in the full cell configuration. The edge effect was avoided by using a negative electrode with a radius 1 mm larger than the radius of the cathode electrode.[23–25] In such configurations, this larger electrode area is available for lithium deposition, which results in lithium deposits over the size of the cathode. Lately, Lee *et al.*[27] correlated the size of counter electrode and the lack of compressive force to the preferable dendritic growth and formation of detached lithium at the boundary of geometric area. It was shown that minimizing pressure free space volume by configuration modification, the dendritic growth and formation of detached lithium is suppressed at the edge.

[a] Dr. J. Bobnar, Dr. A. Vizintin, G. Kapun, Prof. R. Dominko
National Institute of Chemistry
Hajdrihova 19, SI-1001, Ljubljana, Slovenia
E-mail: robert.dominko@ki.si
[b] Dr. J. Bobnar, Prof. R. Dominko, Prof. B. Genorio
University of Ljubljana
Faculty of Chemistry and Chemical Technology
Večna pot 113, SI-1001, Ljubljana, Slovenia
E-mail: bostjan.genorio@fkkt.uni-lj.si
[c] Dr. C. Njel, Prof. R. Dedryvère
CNRS/Univ. Pau & Pays Adour
Institute of Analytical Sciences and Physical Chemistry for Environment and Materials
IPREM-UMR 5254, 64000, Pau, France
[d] Dr. C. Njel, Prof. R. Dedryvère, Prof. R. Dominko
ALISTORE-European Research Institute
33 rue Saint-Leu, Amiens 80039 Cedex, France

Supporting information for this article is available on the WWW under https://doi.org/10.1002/batt.202000255

Contrary to previous studies, it was suggested to use smaller counter electrode to minimize pressure free space. In such configuration, this smaller size of lithium electrode in full cell configuration can lead to undesired etching of the edge of electrode and consequently lowering the active surface area. Further, half-cells are frequently found to contain substrates larger than counter electrode that not filling the entire coin cell; accordingly, there are few reports that crimped separator[10] or gasket[29] was used to define effective area of substrate more accurately (in the size of counter electrode). Rupp *et al.*[29] showed that sodium dendrites on the substrate from the half-cell without a gasket are beyond the edge of the counter electrode. However, most reports use the Li-symmetrical cells to demonstrate the improved electrochemical performance of the engineered lithium metal electrodes.[30] Interestingly, no attention or consideration was given to the edge effect in the Li-symmetrical cell configuration with the same size of working and counter electrode. This motivated us to approach this problem systematically.

In this work, we show how the electrochemically active edges of the electrodes influence the electrochemical results in the Li-symmetrical cell, especially when artificial SEI is formed at the lithium surface. For the model system we used trimethylolpropane ethoxylate triacrylate (TMPETA) polymer protected lithium metal electrodes in a Li-symmetrical cell and performed electrochemical lithium deposition and stripping. The TMPETA polymer (p-TMPETA) with Li-ion conductive additives has already been investigated in some previous research reports in the field of polymer electrolytes in Li-ion batteries.[31–35] To support electrochemical results, electron microscopy (SEM and FIB-SEM), X-ray photoelectron spectroscopy (XPS) and Fourier transform infrared spectroscopy (FTIR) were used. Finally, we proposed a technical solution to overcome the edge effect problem by using a new cell configuration with a polypropylene disc that blocks the Li-ion flow at the edges of the electrodes and limits the electrochemical activity only on the central part of the electrode surfaces. The present study has shown that the results obtained with our technical solution can differ considerably from the results obtained with classical cell configurations. In this respect, we believe that this work is a valuable contribution to improved testing methodology not only in symmetrical cell but more general in cells where metallic lithium is considered as a negative electrode.

Experimental Section

Materials

Trimethylolpropane ethoxylate triacrylate monomer (TMPETA) was obtained from Aldrich (28961-43-5). Lithium foil was purchased from FMC Corporation. Custom-made electrolyte for Li-symmetrical cells was prepared from *bis*(trifluoromethane)sulfonamide lithium salt (LiTFSI, Aldrich, Lot#MKBZ1840 V, 99.95 %), dried under reduced pressure at 150 °C for 24 h, triethylene glycol dimethyl ether (TEGDME, Lot#10199661, Alfa Aesar, 99 %), and 1,3 dioxolane (DOL, Lot#34796TKV, Sigma Aldrich, anhydrous, 99.8 %) both dried with a Na/K alloy and freshly distilled. The measured water content by KF after drying TEGDME and DOL with a Na/K alloy was 1.7 ppm for TEGDME and 0.2 ppm for DOL.

Preparation of p-TMPETA@Li

Lithium foil (500 μm) was scratched with tweezers, roll-pressed with a PP-cylinder and punched into 18 mm diameter size discs. The pure TMPETA or 0.5 vol % TMPETA solution in DOL (V/V) was applied to the lithium surface by drop-casting (40 $\mu L\,cm^{-2}$) and further polymerized at 130 °C for 4 h. The as prepared p-TMPETA-protected lithium discs were punched into the electrodes with a diameter of 14 mm.

SEM characterization

A field-emission scanning electron microscope (FE SEM Supra 35 VP Carl Zeiss) equipped with an energy dispersive X-ray spectrometer INCA Energy 400 (Qxford, UK) was used to obtain SEM images. of the morphology of the p-TMPETA@Li electrodes. Samples were prepared in an argon-filled glovebox and transferred in a custom-made vacuum transfer holder, which is opened in the SEM chamber under reduced pressure.

Cross-sectional analysis was completed using a focused-ion beam – scanning electron microscope (FIB-SEM Helios Nanolab 650i) equipped with an energy dispersive spectrometer (X-Max 50). Initially, the surface was protected with *in situ* deposited platinum to protect the surface and prevent a curtaining effect. Samples were prepared in an argon-filled glovebox and transferred into the microscope chamber under an argon atmosphere.

XPS analysis

To prevent any sample from moisture/air exposure on the analysis site, the samples were removed from their packaging within an argon-filled glovebox (concentration of $O_2 < 0.5$ ppm; concentration of water < 0.5 ppm) and placed onto the sample holder without contamination. After the electrochemical deposition/stripping test, all samples were washed by DOL in baths for 1 min four times (less than 0.4 ppm of water content) to reduce the amount of salt on the surface of the samples. XPS analyses were carried out with a Kratos Axis ultra-spectrometer using focused monochromatized Al $K\alpha$ radiation ($h\nu = 1486.6$ eV). The spectrometer was calibrated using the Ag $3d_{5/2}$ photoemission peak with a full width at half-maximum (FWHM) of 0.58 at 368.3 eV (binding energy), and each photoemission spectrum was recorded with a constant pass energy of 20 eV. The pressure in the analysis chamber was maintained at $\sim 5 \times 10^{-9}$ mbar, and the analyzed area of the samples was $300 \times 700\ \mu m^2$. Short-scan spectra were measured before and after the usual long-scan experiment to check for possible degradation of the samples' surfaces due to exposure from the X-ray beam. The binding-energy scale was calibrated from the hydrocarbon contamination using the C1s peak at 285 eV. The core peaks were analyzed using a nonlinear Shirley-type background and the peak positions and areas were obtained by using a weighted least-squares fitting of model curves (70 % Gaussian, 30 % Lorentzian) to the experimental data. Quantification was performed based on Scofield's relative sensitivity factors.

Electrochemical characterization

All Li-symmetrical cells were assembled in an argon-filled glovebox and all electrochemical measurements were carried out by a Biologic VMP-300 galvanostat/potentiostat at room temperature. Coin cells (type CR2032) were assembled with a manual crimper

(Hohsen Corporation) and disassembled with a coin cell disassembling tool (Hohsen Corporation) for the post-mortem analyses.

Classical Li-symmetrical cells were assembled with two layers of Celgard 2320 (16 mm diameter size) and 1 M LiTFSI in a solvent mixture of TEGDME and DOL with a volume ratio of 1:1 (10 μL per cell; 3.3 μL per cm^2 of available active lithium on the start). As working and counter electrodes (14 mm diameter size) were used, p-TMPETA@Li or non-protected lithium.

New Li-symmetrical cell configuration combined a layer of Celgard 2320 (16 mm), PP disc with 2 layers of Celgard 2320 (8 mm) in the gap and with an additional layer of Celgard 2320 (16 mm) as separator, non-protected lithium or p-TMPETA@Li as both working and counter electrodes (14 mm diameter size). The 1 M LiTFSI in a solvent mixture of TEGDME and DOL with a volume ratio of 1:1 was used as electrolyte (14 μL per cell; 14 μL per cm^2 of available active lithium on the start). PP discs were specially fabricated from 50 μm thick, non-porous PP sheet by cutting 16 mm diameter discs with 8 mm diameter gap in the center.

Li-symmetrical cells were examined with two different tests. First: Li-symmetrical cells were activated in the 1st cycle by deposition/stripping with a current density of 0.5 mA cm^{-2} for 4 h corresponding to a specific capacity of 2 mAh cm^{-2} and followed by deposition/stripping with a current density of 0.5 mA cm^{-2} for 2 h corresponding to a specific capacity of 1 mAh cm^{-2}. Second: Li-symmetrical cells were cycled at current density of 2.0 mA cm^{-2} for 2.5 h corresponding to a specific capacity of 5 mAh cm^{-2}.

2. Results and Discussion

2.1. Preparation of Model Protective Layer on Lithium Surface with Restricted Li-Ion Conductivity

In order to strongly impede the electrolyte transport to the lithium surface, trimethylolpropane ethoxylate triacrylate (TMPETA) was used as a precursor of the protective layer on the lithium surface. Furthermore, no additional Li-ion conductive additives were used. p-TMPETA was prepared by *in situ* anionic polymerization on the lithium surface, with lithium acting as initiator of the polymerization (Figure 1a, Figure S1 in the Supporting Information). To strongly reduce the TMPETA load on the lithium surface, the TMPETA was dissolved in 1,3-dioxolane (DOL) (0.5 vol% solution) and *in situ* polymerized on the lithium surface (p-TMPETA@Li). The polymerization of TMPETA on the lithium surface was confirmed by XPS (Figure S2) and FTIR analysis (Figure S3). In addition, surface morphology of pristine lithium and the morphology of p-TMPETA@Li was evaluated and compared by SEM. Figure 1b shows the morphology of pristine lithium with conventional ripple marks on its surface. When the p-TMPETA layer was prepared on the lithium surface (Figure 1d), these ripple marks appear to be covered by an adhesive-like layer. However, these ripple marks may be visible through the p-TMPETA layer. The thickness of p-TMPETA@Li (40 μL cm^{-2} loading) was evaluated by cross-sectional SEM analysis and was between 200–300 nm

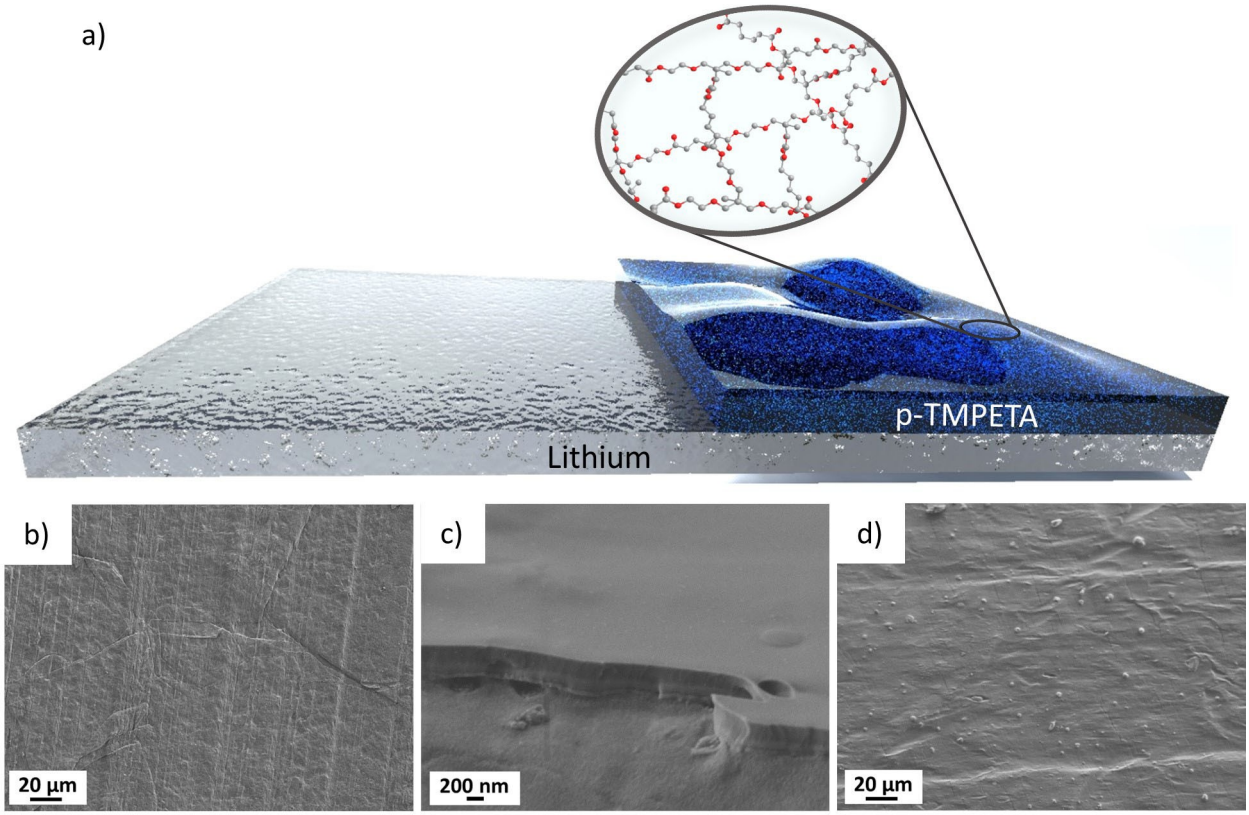

Figure 1. a) Scheme of p-TMPETA on lithium metal surface (p-TMPETA@Li) and corresponding SEM images of the b) pristine non-protected lithium metal, c) cross-section of p-TMPETA@Li, and d) top-down view of p-TMPETA@Li.

(Figure 1c). So prepared surfaces were used in electrochemical studies in classical Li-symmetrical cells.

2.2. Electrochemical Evaluation in a Classical Li-Symmetrical Cell Configuration

The classical Li-symmetrical cell consists of two lithium metal electrodes and a separator soaked with an electrolyte (Figure 2a). Here we have used such a cell which consists of lithium metal electrodes with a diameter of 14 mm, 2 layers of Celgard 2320 with a diameter of 16 mm and 1 M LiTFSI in the solvent mixture tetraglyme (TEGDME):DOL with a volume ratio of 1:1 (10 μL per cell; 3.3 μL per cm^2 of available active lithium on the start). It is worth noting that the diameter of the separator is larger than that of the lithium metal electrodes to avoid short circuits at the edges due to poor coverage. In such a cell configuration the electrochemical behavior of non-protected lithium and p-TMPETA@Li electrodes was investigated at two different current densities: 0.5 mA cm^{-2} and 2 mA cm^{-2}. At a current density of 0.5 mA cm^{-2} (Figure 2b), the overpotential for a Li-symmetrical cell with non-protected lithium increases

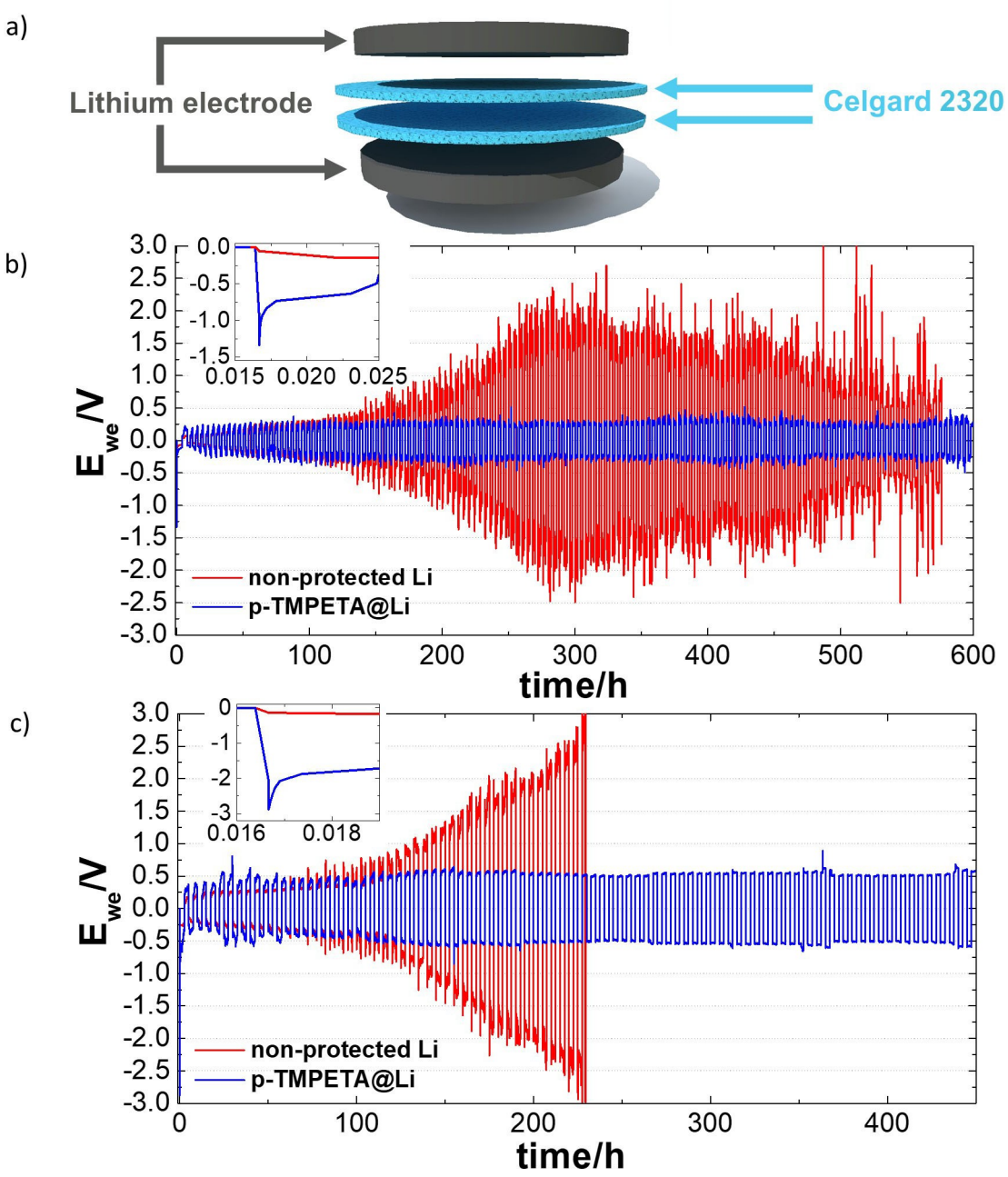

Figure 2. a) Scheme of the classical Li-symmetrical cell configuration with corresponding electrochemical curves for non-protected lithium and p-TMPETA@Li classical Li-symmetrical cells with inset of a corresponding zoomed area at a current density of b) 0.5 mA cm^{-2} and c) 2 mA cm^{-2}. In all experiments the electrolyte quantity was 3.3 μL per cm^2 of available active lithium on the start.

rapidly and reaches more than 2 V after 300 h of deposition/stripping cycling. This rapid increase in overpotential is related to the limited amount of electrolyte and its consumption for irreversible reactions on the lithium surface due to the presence of unstable SEI. The p-TMPETA@Li symmetrical cell showed an increased overpotential in the initial half cycle (1.4 V) and was significantly higher compared to non-protected Li-symmetrical cell (0.16 V) (Figure 2b). In the second half cycle, the overpotential was reduced to values similar to those of the symmetrical cell with non-protected lithium, indicating that ion transport corridors were established. In contrast to the symmetrical cell with non-protected lithium, the symmetrical cell with p-TMPETA@Li showed a stable cycling behavior with almost no increase of overpotential for more than 600 h.

At a higher current density of 2 mA cm^{-2} (Figure 2c), the overpotential of non-protected Li-symmetrical cell increased even faster and reached the cut-off voltage (3 V) after 227 h of deposition/stripping cycling. On the other hand, p-TMPETA@Li showed a much more stable cycling behavior with significantly lower overpotential even after 400 h of cycling compared to symmetrical cell with non-protected lithium. With increased current density, however, an increased overpotential in the first half-wave cycle can also be observed in symmetrical cells with p-TMPETA@Li, which reached 2.8 V and is significantly higher than in symmetrical cells with non-protected lithium (0.34 V). However, in the second half cycle p-TMPETA@Li symmetrical cells have a similar overpotential as symmetrical cells with non-protected lithium. From these results we can conclude that p-TMPETA is stable and can withstand the stress caused by the volume change of lithium during the deposition/stripping process, which is manifested by the suppression of electrolyte consumption for irreversible reactions and a more stable overpotential during the cycling.

Post-mortem analyses were performed on electrodes recovered from classical Li-symmetrical cells after 300 h of deposition/stripping cycling at current density of 0.5 mA cm^{-2}. SEM comparison of electrode morphology and XPS C1s composition of non-protected lithium and p-TMPETA@Li electrodes-before and after cycling were done (Figure 3). It can be clearly seen that non-protected lithium is significantly corroded, showing irregular surface morphology over the entire surface (Figure 3a). Irregular surface morphology is additionally a consequence of a HSAL growth (Figure 3b). In contrast, most of the p-TMPETA@Li surface was preserved, but the edge portion of the electrode is similarly rough and corroded as the surface of non-protected lithium after cycling (Figure 3c, d, e). In the following step the

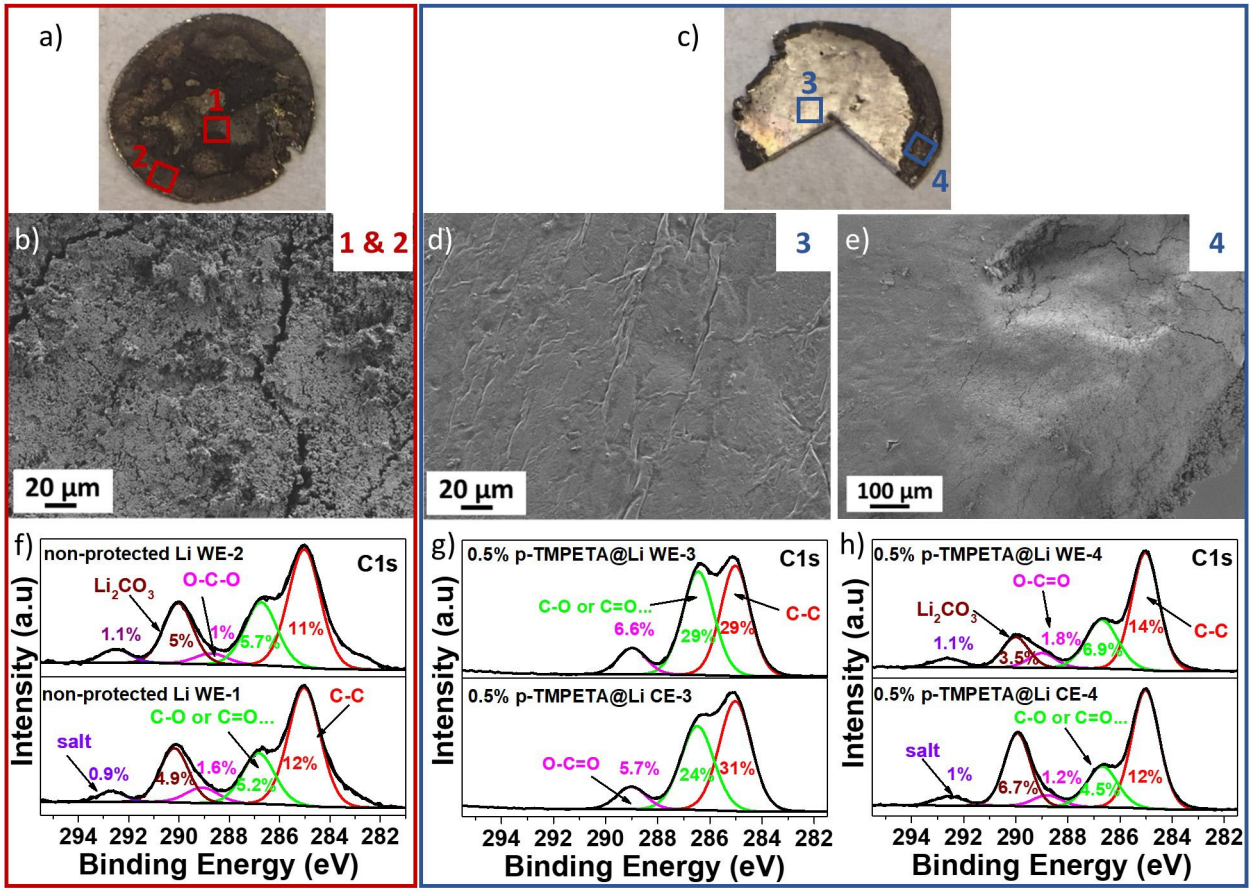

Figure 3. a) Photograph of non-protected lithium after 300 h of cycling in classical Li-symmetrical cell at current density of 0.5 mA cm^{-2} with corresponding b) SEM image. c) Photograph of p-TMPETA@Li after 300 h of cycling in classical Li-symmetrical cell with corresponding SEM image of d) central part (3) and e) edge part (4) of electrode. Corresponding XPS C1s spectra of f) non-protected lithium, g) central part (3) of p-TMPETA@Li, and h) edge part (4) of p-TMPETA@Li.

electrode surfaces were post-mortem analyzed by the XPS to assess the salt degradation species from the electrolyte (Figure 3). The XPS analysis was performed in two different regions; the central part and edge part - ring of the electrodes. The C1s core level signal shows a similar composition over the entire surface (central (1) and edge part (2)) for non-protected lithium electrode (Figure 3f). In contrast, C1s core level signal of p-TMPETA@Li shows significantly different composition in the central part (3) compared to edge part (4) of WE and CE (Figure 3g, h). The XPS confirmed preserved central part (3) of p-TMPETA@Li electrodes (working (WE) and counter electrode (CE)) with similar carbon environment (presence of p-TMPETA "finger-print" signal) as found on as prepared p-TMPETA@Li (Figure S2b). However, the corroded edge part of p-TMPETA@Li electrodes had a similar composition to corroded non-protected lithium with the presence of Li_2CO_3 and other electrolyte degradation products. The correlation between XPS and the SEM analysis suggests two different scenarios. In the first case, the p-TMPETA protective layer successfully suppressed HSAL growth in the central part of the electrode. However, during lithium deposition/stripping, some imperfections were formed at the edges where a similar morphology and composition to the non-protected lithium electrode was found. Secondly, the results obtained clearly show that most of the electrochemical deposition/stripping occurred only at the edge part of the p-TMPETA@Li electrode, while the central part remained intact. This behavior can be attributed to very thick artificial p-TMPETA@Li layers (approx. 7930 layers; Figure S1) and consequently to the impermeability that hindered the vertical Li-ion mass transport to the lithium surface.

In addition, the FIB-SEM was used to study lithium morphology under the p-TMPTEA layer after cycling (Figure 4a). For this purpose, the FIB-SEM cross-sectional comparison was performed between the as prepared p-TMPETA@Li, cycled non-protected lithium and cycled p-TMPETA@Li (Figure 4 and Figure S4). The cross-section in Figure 4b clearly shows that 300 h of deposition/stripping cycling result in a porous HSAL structure as known from the literature.[36] As prepared p-TMPETA@Li is shown in Figure 4c. A compact Li structure under the p-TMPETA layer (black line) that corresponds to the pristine lithium metal morphology[36] is preserved after 300 h of cycling (Figure 4d). This intact lithium morphology indicates that there was no vertical diffusion of Li-ions through the p-TMPETA layer; this means that only the edge of the electrode was involved in the lithium deposition/stripping cycling. It was previously shown that the diffusion processes play one of the key roles in understanding the change in morphology on a given surface. DFT calculations showed that the self-diffusion barriers of lithium on lattice planes are very high (Li(001): 0.14 eV, Li(111): 0.41 eV).[37] This indicates that even in the idealistic case of a monocrystalline lithium surface, the high diffusion barriers would hinder epitaxial growth (i.e. the growth of monolayers); lithium therefore always shows a tendency to have a rough surface morphology and to form HSAL. Considering DFT from literature[37] and our FIB-SEM results, we concluded that the p-TMPETA layer is impermeable to Li-ion transport, therefore the central part of the electrode was not involved in the electrochemical deposition/stripping process.

Furthermore, the results obtained clearly show that lithium striping and deposition occurs only at the edge of p-TMPETA@Li electrodes. Consequently, the obtained electrochemical results of classical symmetrical cells do not show the actual protective character of the artificial SEI but rather an edge effect mentioned in the introduction. This was the motivation to design and develop a new symmetrical cell configuration.

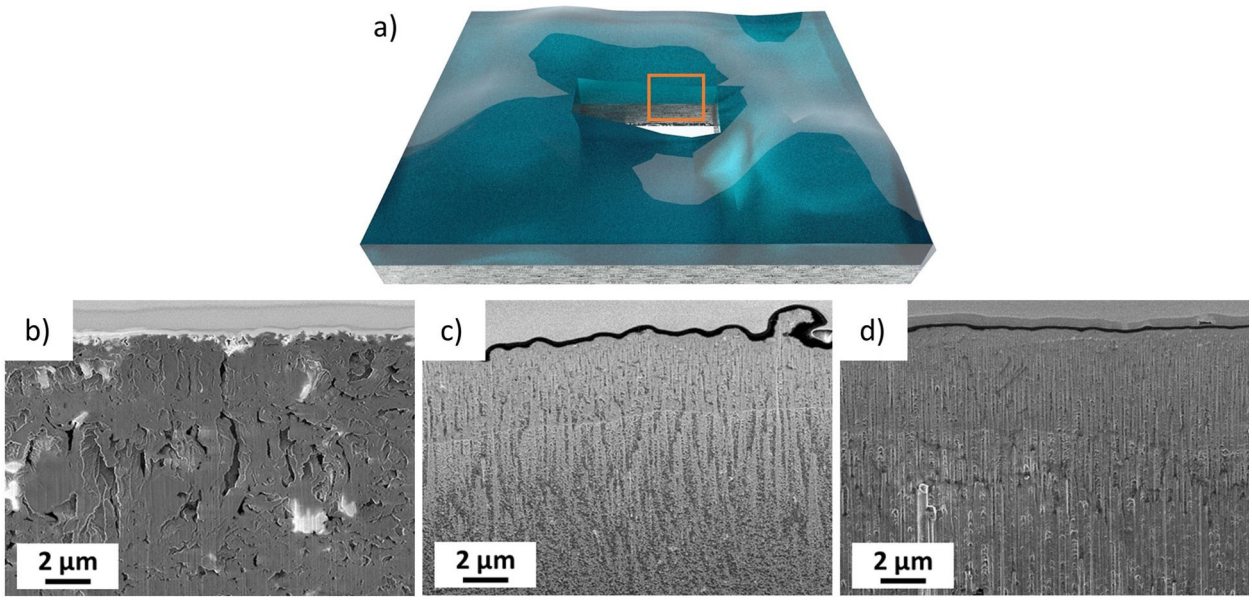

Figure 4. a) Schematic of FIB-SEM cross-sections and FIB-SEM images of b) non-protected lithium after 300 h in classical Li-symmetric cell, c) pristine 0.5% p-TMPETA@Li and d) 0.5% p-TMPETA@Li after 300 h in classical Li-symmetric cell.

2.3. Electrochemical Evaluation in a New Li-Symmetrical Cell Configuration

To eliminate the edge effect, we have designed a new cell configuration (Figure 5a) that allows the deposition/stripping process to be tested over the selected area of the electrode, excluding the edge. Accordingly, we have designed a 50 μm thick disc of non-porous polypropylene (PP) with gap. Due to the non-porous structure of the disc and the non-wetting properties in an ether-based electrolyte, the lateral Li-ion transport should be reduced and thus the edge effect should be prevented. In addition, the PP disc is chemically stable within the Li-symmetrical cell and thus has no influence on the electrochemical deposition/stripping process (Figure S6). In this new cell configuration, two layers of Celgard 2320 were introduced into PP disc gap. The electrolyte was evenly distributed between the Celgard 2320 layers with a total volume of 14 μL (7 μL per cm^2 of separator surface).

To test the efficiency of the new cell configuration, electrochemical deposition/stripping was performed at a current density of 0.5 mA cm^{-2} using non-protected lithium and p-TMPETA@Li electrodes (Figure 5b) and compared to the classical cell configuration (Figure 2b). The non-protected lithium in the new symmetrical cell configuration showed a similar behavior as in the classical cell configuration with an overpotential of a similar magnitude (Figure 2b and Figure 5b). In contrast, the overpotential of the new symmetrical cell with p-TMPETA@Li was drastically increased and reached a cut-off voltage of 3 V in the first half cycle. Consequently, the desired amount of lithium was not transferred between the electrodes. The achieved cut-off voltage is most-likely due to the extremely high resistance of the p-TMPETA layer. We assume that the artificial SEI is almost impermeable and hinders the vertical Li-ion mass transfer through the p-TMPETA layer. The overpotential decreased in the next two cycles, but the monotonic increase of the overpotential was observed with further continuous cycling. Interestingly, the overpotential of the new symmetrical cell with non-protected lithium did not overcome the overpotential of the symmetrical p-TMPETA@Li cell as observed in the classical cell configuration without edge shielding. A visible asymmetric increase of the overpotential (Figure 5b) could be correlated with the inhomogeneity of the p-TMPETA layer on lithium and the induced imperfections during the electrochemical cycling. However, a more symmetrical overpotential was shown for continuous cycling. Furthermore, the arc-like shape of deposition/stripping curve

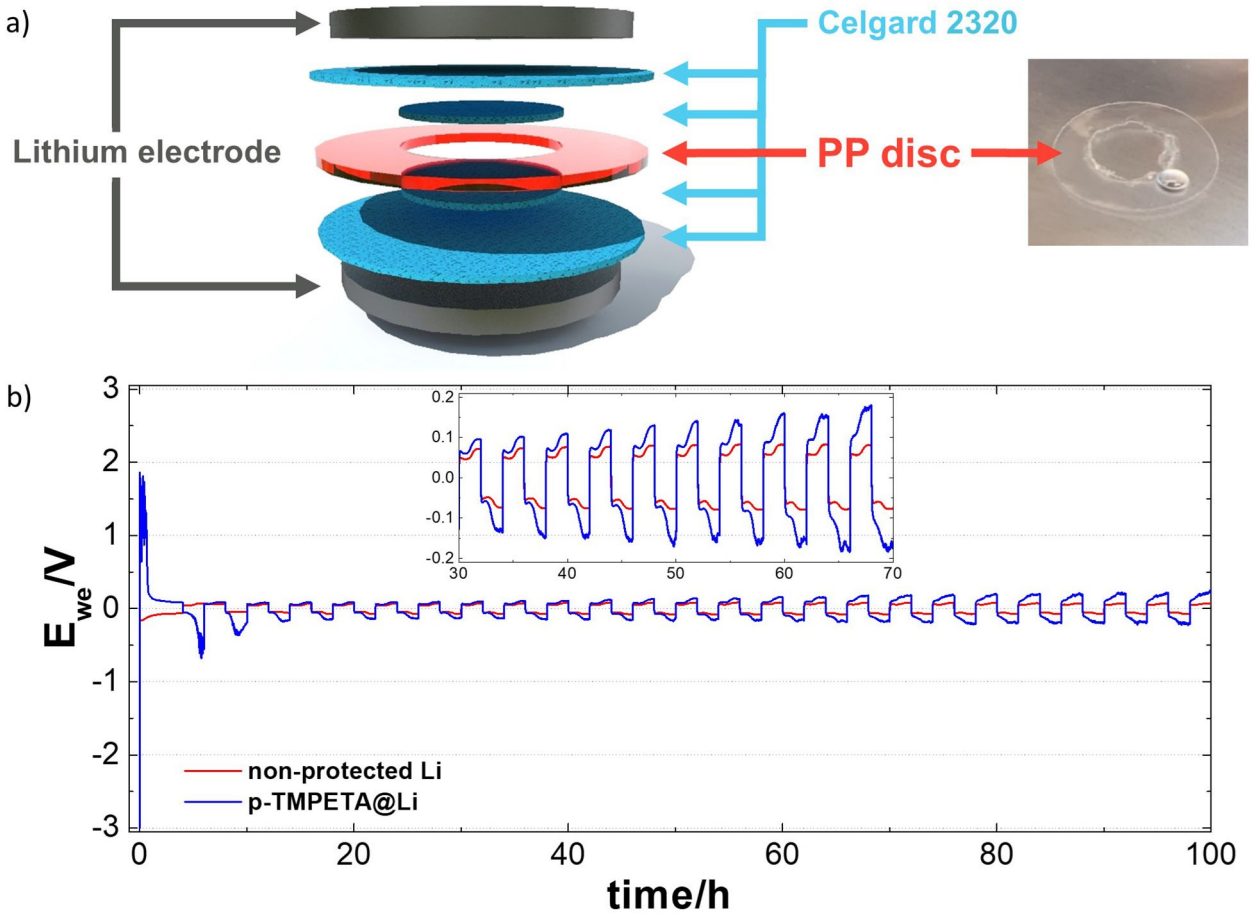

Figure 5. a) Schematic presentation of the new Li-symmetrical cell configuration with optical image of the PP disc. b) Electrochemical deposition/stripping behavior of the new Li-symmetrical cell at a current density of 0.5 mA cm^{-2} for non-protected lithium and p-TMPETA@Li with inset of enlarged area from 30 to 70 h of cycling. In all experiments the electrolyte quantity was 14 μL per cm^2 of available active lithium on the start.

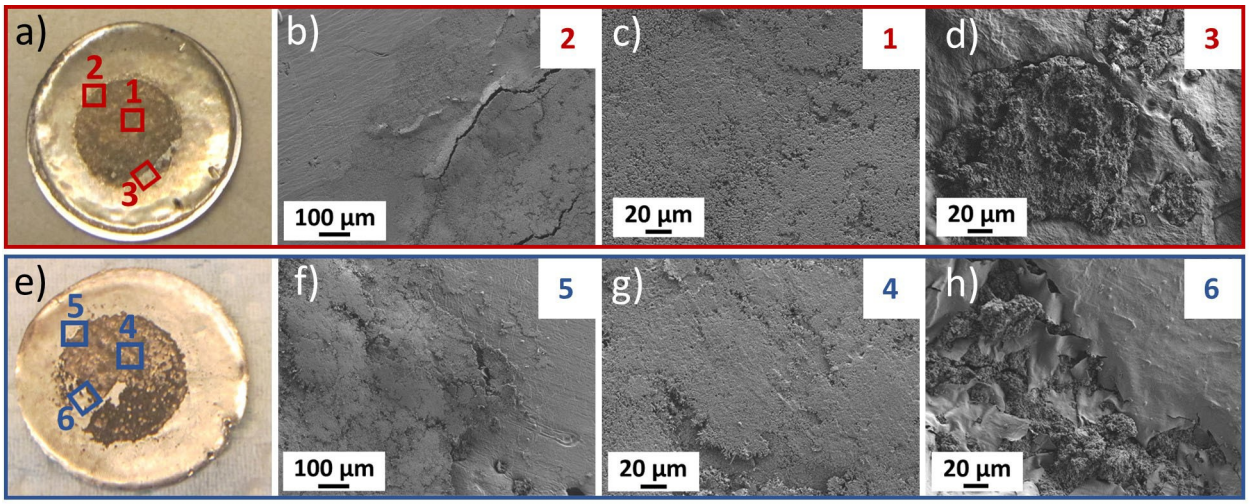

Figure 6. a) Optical images of recovered non-protected lithium electrode from new Li-symmetrical cell with corresponding SEM images of b) edge of the limited active electrode surface (2), c) central part of electrode (1) and d) surface under detached Li and HSAL (3). e) Photograph of recovered p-TMPETA@Li electrode from new Li-symmetrical cell after 100 h of cycling with corresponding SEM images of f) edge of the limited active electrode surface (2), g) central part of electrode (1) and h) surface under detached Li and HSAL (3).

could be a consequence of the restricted Li-ion transfer through the p-TMPETA layer, as known from the literature.[38]

Furthermore, post-mortem analysis was performed on the new Li-symmetrical cells configuration after 100 h deposition/stripping test. The limited cycling area (dark grey corroded surface) is clearly visible and had the same size as the gap in the PP disc (Figure 6a). The SEM analysis confirmed limited cycled area achieved by new cell configuration (Figure 6b). Further, similar HSAL growth is visible in the cycled area (Figure 6c) as observed on non-protected lithium electrode from classical Li-symmetrical cell (Figure 3b). In addition, cracking of the SEI, caused by dendritic growth may be visible under the HSAL morphology (Figure 6d). The overall result shows that the use of a PP disc allowed a more precisely defined effective area with homogeneously distributed current density without a so-called edge effect. Such a configuration was manifested by more accurate deposition/stripping curves in terms of surface electrochemistry.

The photograph of p-TMPETA@Li electrode after 100 h of cycling in a symmetrical cell with PP disc are shown in Figure 6e. This electrode showed similarly corroded surfaces in a limited cycling area after cycling as obtained on the non-protected lithium (Figure 6a). Furthermore, a limited cycling area was also confirmed on the p-TMPETA@Li electrode by SEM (Figure 6f). Interestingly, after avoiding edge effect, a similar HSAL morphology (Figure 6g) with islands in which the p-TMPETA (Figure 6h) is cracked is visible on the cycled area of the p-TMPETA@Li electrode. By limiting the cycling area (use of PP disc) and thus avoiding the edge effect, it was shown that p-TMPETA@Li does not exhibit improved cycling performance and that the p-TMPETA layer does not have a protective effect as we initially anticipated. This conclusion could not be made by classical Li-symmetrical cell configuration since it gave false results. Such a finding indicates that appropriate design of the symmetrical cell is of great importance and must be adopted in order to understand deposition/stripping of lithium underneath the artificial SEI.

3. Conclusions

We have shown how important it is to be aware of potentially hindered Li-ion transport from an electrolyte to a lithium surface when a protective layer or artificial SEI is used on the lithium surface. Obstructed Li-ion transport to a lithium surface can significantly intensify the edge effect, which can easily lead to a misinterpretation of the protective layer nature. In order to avoid the edge effect, we have developed and tested the new cell configuration with PP disc with gap, which allows a simple electrochemical evaluation of the artificial SEI or protective layer and its effects on striping and deposition. The purpose of the proposed new cell configuration is to provide a more precisely defined effective area with homogeneously distributed current density without edge effect and more accurate deposition/stripping curves related to surface electrochemistry. Furthermore, such a technology solution, the protection of the edge of electrode with PP disk/layer, might be of interest for companies processing protected lithium electrodes, where the trimming of the edges occurs after the protection layer is applied on the surface of the lithium electrode.

Acknowledgments

This work is supported by the HELiS project which receives funding from the European Union's Horizon 2020 research and innovation program under Grant Agreement No 666221 and from the Slovenian Research Agency research programs P1-0112 and P2-0393.

Conflict of Interest

The authors declare no conflict of interest.

Keywords: artificial solid-electrolyte interphase · edge effect · lithium metal batteries · new cell configuration · symmetrical cell

[1] C. Yang, K. Fu, Y. Zhang, E. Hitz, L. Hu, *Adv. Mater.* **2017**, *29*, 1701169.
[2] W. Xu, J. Wang, F. Ding, X. Chen, E. Nasybulin, Y. Zhang, J.-G. G. Zhang, *Energy Environ. Sci.* **2014**, *7*, 513–537.
[3] Y. Guo, H. Li, T. Zhai, *Adv. Mater.* **2017**, *29*, 1700007.
[4] D. Lin, Y. Liu, Y. Cui, *Nat. Nanotechnol.* **2017**, *12*, 194–206.
[5] M. Barghamadi, A. S. Best, A. I. Bhatt, A. F. Hollenkamp, P. J. Mahon, M. Musameh, T. Rüther, *J. Power Sources* **2015**, *295*, 212–220.
[6] S. J. Choi, S. H. Lee, Y. C. Ha, J. H. Yu, C. H. Doh, Y. Lee, J. W. Park, S. M. Lee, H. C. Shin, *J. Electrochem. Soc.* **2018**, *165*, A952–A962.
[7] W.-K. Shin, A. G. Kannan, D.-W. Kim, *ACS Appl. Mater. Interfaces* **2015**, *7*, 23700–23707.
[8] W. Luo, L. Zhou, K. Fu, Z. Yang, J. Wan, M. Manno, Y. Yao, H. Zhu, B. Yang, L. Hu, *Nano Lett.* **2015**, *15*, 6149–6154.
[9] J. Bobnar, M. Lozinšek, G. Kapun, C. Njel, R. Dedryvère, B. Genorio, R. Dominko, *Sci. Rep.* **2018**, *8*, 5819.
[10] Y. Liu, D. Lin, P. Y. Yuen, K. Liu, J. Xie, R. H. Dauskardt, Y. Cui, *Adv. Mater.* **2017**, *29*, 1605531.
[11] N. Delaporte, Y. Wang, K. Zaghib, *Front. Mater.* **2019**, *6*, DOI 10.3389/fmats.2019.00267.
[12] Y. J. Zhang, X. Y. Liu, W. Q. Bai, H. Tang, S. J. Shi, X. L. Wang, C. D. Gu, J. P. Tu, *J. Power Sources* **2014**, *266*, 43–50.
[13] G. Zheng, S. W. Lee, Z. Liang, H.-W. Lee, K. Yan, H. Yao, H. Wang, W. Li, S. Chu, Y. Cui, *Nat. Nanotechnol.* **2014**, *9*, 618–623.
[14] G. Ma, Z. Wen, Q. Wang, C. Shen, J. Jin, X. Wu, *J. Mater. Chem. A* **2014**, *2*, 19355–19359.
[15] S. M. Choi, I. S. Kang, Y.-K. Sun, J.-H. Song, S.-M. Chung, D.-W. Kim, *J. Power Sources* **2013**, *244*, 363–368.
[16] M. Buonaiuto, S. Neuhold, D. J. Schroeder, C. M. Lopez, J. T. Vaughey, *ChemPlusChem* **2015**, *80*, 363–367.
[17] K. Naoi, M. Mori, M. Inoue, T. Wakabayashi, K. Yamauchi, *J. Electrochem. Soc.* **2000**, *147*, 813–819.
[18] K. Chung, W.-S. Kim, Y.-K. Choi, *J. Electroanal. Chem.* **2004**, *566*, 263–267.
[19] R. Xu, Y. Xiao, R. Zhang, X. Cheng, C. Zhao, X. Zhang, C. Yan, Q. Zhang, J. Huang, *Adv. Mater.* **2019**, *31*, 1808392.
[20] A. La Monaca, A. Paolella, A. Guerfi, F. Rosei, K. Zaghib, *Electrochem. Commun.* **2019**, *104*, 106483.
[21] D. J. Lee, H. Lee, J. Song, M.-H. Ryou, Y. M. Lee, H.-T. Kim, J.-K. Park, *Electrochem. Commun.* **2014**, *40*, 45–48.
[22] H.-K. Jing, L.-L. Kong, S. Liu, G.-R. Li, X.-P. Gao, *J. Mater. Chem. A* **2015**, *3*, 12213–12219.
[23] A. Ferrese, P. Albertus, J. Christensen, J. Newman, *J. Electrochem. Soc.* **2012**, *159*, A1615–A1623.
[24] J. Yamaki, S. Tobishima, Y. Sakurai, K. Saito, K. Hayashi, *J. Appl. Electrochem.* **1998**, *28*, 2–7.
[25] M. Tang, P. Albertus, J. Newman, *J. Electrochem. Soc.* **2009**, *156*, A390–A399.
[26] M. Golozar, A. Paolella, H. Demers, S. Bessette, M. Lagacé, P. Bouchard, A. Guer, R. Gauvin, K. Zaghib, *Nat. Commun.* **2019**, 1–9.
[27] H. Lee, S. Chen, X. Ren, A. Martinez, V. Shutthanandan, M. Vijayakumar, K. S. Han, Q. Li, J. Liu, W. Xu, J.-G. Zhang, *ChemSusChem* **2018**, *11*, 3821–3828.
[28] J. Cannarella, C. B. Arnold, *J. Electrochem. Soc.* **2015**, *162*, A1365–A1373.
[29] R. Rupp, A. Vlad, *J. Electrochem. Soc.* **2019**, *166*, A3122–A3131.
[30] D. Koo, B. Kwon, J. Lee, K. T. Lee, *Chem. Commun.* **2019**, *55*, 9637–9640.
[31] E.-H. Kil, H.-J. Ha, S.-Y. Lee, *Macromol. Chem. Phys.* **2011**, *212*, 2217–2223.
[32] S.-I. Kim, H.-S. Kim, S.-H. Na, S.-I. Moon, Y.-J. Kim, N.-J. Jo, *Electrochim. Acta* **2004**, *50*, 317–321.
[33] K.-H. Choi, S.-H. Kim, H.-J. Ha, E.-H. Kil, C. K. Lee, S. B. Lee, J. K. Shim, S.-Y. Lee, *J. Mater. Chem. A* **2013**, *1*, 5224.
[34] S.-H. Kim, K.-H. Choi, S.-J. Cho, E.-H. Kil, S.-Y. Lee, *J. Mater. Chem. A* **2013**, *1*, 4949.
[35] K.-H. Choi, S.-J. Cho, S.-H. Kim, Y. H. Kwon, J. Y. Kim, S.-Y. Lee, *Adv. Funct. Mater.* **2014**, *24*, 44–52.
[36] J. Z. Lee, T. A. Wynn, M. A. Schroeder, J. Alvarado, X. Wang, K. Xu, Y. S. Meng, *ACS Energy Lett.* **2019**, *4*, 489–493.
[37] M. Jäckle, A. Groß, *J. Chem. Phys.* **2014**, *141*, 174710.
[38] K.-H. Chen, K. N. Wood, E. Kazyak, W. S. LePage, A. L. Davis, A. J. Sanchez, N. P. Dasgupta, *J. Mater. Chem. A* **2017**, *5*, 11671–11681.

Manuscript received: October 28, 2020
Revised manuscript received: December 7, 2020
Accepted manuscript online: December 16, 2020
Version of record online: December 22, 2020